

# Direct measurement of spin-flip rates in single-electron tunneling

Olfa Dani,<sup>1</sup> Robert Hussein,<sup>2</sup> Johannes C. Bayer,<sup>1</sup> Klaus Pierz,<sup>3</sup> Sigmund Kohler,<sup>4</sup> and Rolf J. Haug<sup>1</sup>

<sup>1</sup>*Institut für Festkörperphysik, Leibniz Universität Hannover, D-30167 Hanover, Germany*

<sup>2</sup>*Institut für Festkörpertheorie und -optik, Friedrich-Schiller-Universität Jena, D-07743 Jena, Germany*

<sup>3</sup>*Physikalisch-Technische Bundesanstalt, Bundesallee 100, D-38116 Braunschweig, Germany*

<sup>4</sup>*Instituto de Ciencia de Materiales de Madrid, CSIC, E-28049 Madrid, Spain*

(Dated: February 2, 2024)

Spin-flips are one of the limiting factors for spin-based information processing. We demonstrate a transport approach for determining the spin-flip rates of a self-assembled InAs double quantum dot occupied by a single electron. In such devices, different Landé factors lead to an inhomogeneous Zeeman splitting, so that the two spin channels can never be at resonance simultaneously, leading to a spin blockade at low temperatures. This blockade is analyzed in terms of spin flips for different temperatures and magnetic fields. Our results are in good agreement with a quantum master equation that combines the dot-lead couplings with ohmic dissipation stemming from spin-flip cotunneling.

## I. INTRODUCTION

The concept of quantum computing based on spins in coupled quantum dots was proposed 25 years ago [1] and appears to be within reach of applications nowadays [2–4]. Initialization and control of the spin is critically dependent on the coherence of the spins. A number of theory works showed a sensitive dependence of the spin coherence on the hyperfine coupling [5] or cotunneling [6, 7], as well as on the influence of Markovian [8] or non-Markovian [9] noise. The spin-phonon coupling mediated by spin-orbit interaction is often quite small and the dominating contribution to spin decoherence is generally assumed to happen via hyperfine interaction. Spin relaxation rates were addressed experimentally for single quantum dots [10–15] and also for coupled quantum dots [16–21]. There the decay rate as a function of the Zeeman splitting hints on the dominating dissipation process. In coupled quantum dots, mostly the spin blockade mechanism [16] based on the energetic difference between singlet and triplet two-electron states was studied in such measurements. It was shown that these two-electron states relax the spin predominantly via hyperfine interaction and spin-orbit interaction in III-V semiconductors [22–24], whereas in silicon and germanium dots also cotunneling [25–29] can be of importance. For transport phenomena that depend on the dynamics of a single spin in a double quantum dot only very few studies exist [21, 30, 31].

Here, we demonstrate how to directly extract the spin-flip rates for single spins in coupled quantum dots from the measured single-electron tunneling current. To this end, we use a double quantum dot with a Zeeman level structure similar to the one of Ref. [30], but with an inter-dot tunneling much smaller than the typical detuning. Then, in contrast to this former work, the resulting current blockade is resolved by spin flips. For their theoretical description, we consider spin-flip cotunneling [6, 7], i.e., dissipative spin transitions accompanied by excitations at the Fermi surface of a lead. As a consequence, the spin experiences ohmic dissipation [32, 33] which fits the experimental data rather well, i.e., we show that spin-flip cotunneling is the dominant mechanism for spin relaxation in our double quantum dot occupied by a single electron.

## II. EXPERIMENT

For our investigation, we use vertically coupled self-assembled InAs quantum dots. The quantum dots are embedded in a GaAs-AlAs heterostructure. Due to the lattice-mismatch of InAs and AlAs pyramid-shaped quantum dots are

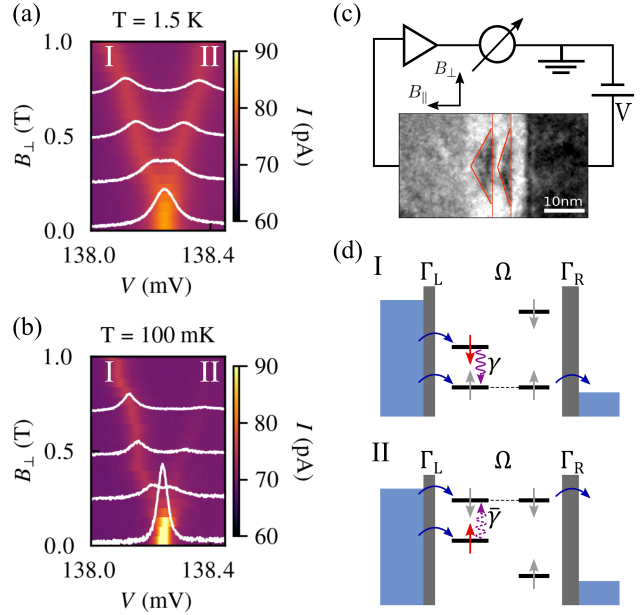


FIG. 1. (a) Current-voltage characteristic of InAs double quantum dots as function of the magnetic field applied perpendicular to the tunneling current up to  $B = 1$  T at  $T = 1.5$  K, showing a current peak at  $V \approx 138.25$  mV for  $B = 0$ . The white lines depict cuts along the color graphs, showing the current peaks for a given magnetic field. (b) Same for  $T = 100$  mK. (c) TEM image of an InAs double quantum dot shown in a schematic picture of the measurement setup and of the different magnetic field directions used. (d) Sketch of the transport channels for the different situations of resonance I and II. Due to the inhomogeneous Zeeman splittings always one channel is off-resonant for the two different resonance conditions. An electron may be trapped in that channel and block transport until a spin flip indicated by the purple arrow brings the electron to the resonant channel.

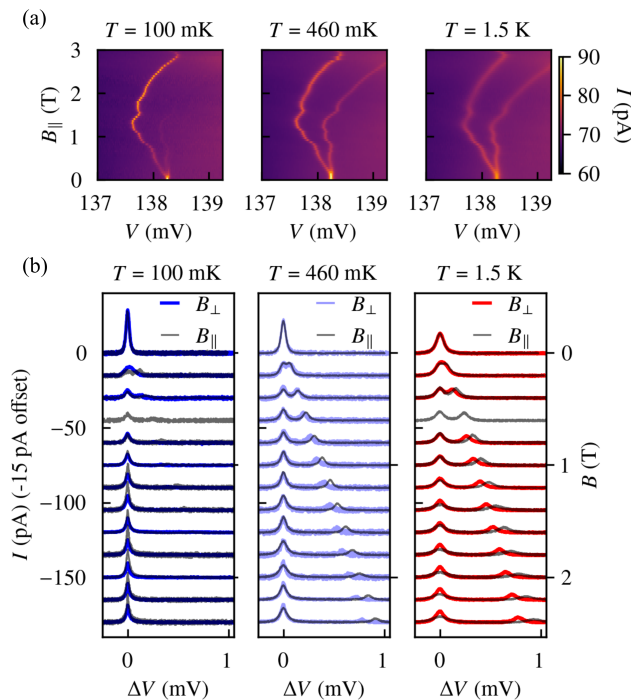


FIG. 2. (a) Magnetic field dependence of the tunneling current as function of voltage for magnetic field applied parallel to the tunneling current for three different temperatures  $T = 100$  mK, 460 mK, and 1.5 K. (b) Tunneling current as function of applied voltage normalized to the position of resonance I for the two different magnetic field directions. Traces offset by  $-15$  pA are shown for magnetic fields ranging from 0 up to 2.4 T in step sizes of 0.2 T.

formed and vertically aligned [34]. The dot in the second layer is slightly larger than the quantum dot in the first one [35] due to the change in strain field. The diameter of such quantum dots typically is 10 to 20 nm and their height is between 2 and 4 nm. In these small dots the strong confinement leads to the Landé  $g$ -factor deviating strongly from the bulk value, approaching  $g = 2$  of the free electron with decreasing dot sizes. The effective thickness of the middle and top barriers is reduced by the quantum dots partially penetrating the AlAs layers, which results in asymmetric dot-lead tunneling rates. A TEM image of such an InAs double quantum dot is depicted in Fig. 1(c). The device is similar to the ones used in Refs. [31, 36, 37], i.e. for zero bias the quantum dot levels are above the Fermi energy and tunneling is not possible whereas for finite bias voltage the quantum dot levels are shifted by the electric field and brought into resonance and into the transport window.

The color graphs in Figs. 1(a,b) show the measured current  $I$  through the InAs double quantum dot as a function of bias voltage  $V$  and magnetic field up to  $B = 1$  T at  $T = 1.5$  K and  $T = 100$  mK, respectively. The magnetic field was applied perpendicular to the current (parallel to the layer structure). The graphs for  $B = 0$  show a current peak at  $V \approx 138.25$  mV  $\equiv V_0$ , owing to the resonant tunneling of single electrons through the InAs double quantum dot. The resonance originates from tunnel cycles with the occupation  $(0, 0) \rightarrow (1, 0) \rightarrow (0, 1)$ ,

where only a single electron is present in the double quantum dot. At  $T = 1.5$  K, the single resonance splits into two peaks (a left peak: peak I and a right peak: peak II) for increasing magnetic field. At  $T = 100$  mK [Fig. 1(b)], the resonant tunneling peak amplitude at  $B = 0$  is higher [31] and decreases drastically already with small magnetic fields  $\sim 0.25$  T applied. The amplitude of peak I stays at a low but finite level with increasing magnetic field, meanwhile the right peak fades away totally.

This observation can be explained by the different effect of spin relaxation as sketched in Fig. 1(d). Due to the different sizes of the two dots, their  $g$ -factors  $g_L$  and  $g_R$  are different and therefore the Zeeman splitting becomes inhomogeneous [38, 39]. For  $V < V_0$  (peak I) the spin-down Zeeman levels of both quantum dots are in resonance, such that we expect to find a current peak. An electron with spin-up, however, entering the left dot will get stuck, because the right dot is off-resonance, such that the resonant channel becomes blocked. This blockade can be resolved by a spin flip with rate  $\gamma$  for all temperatures because it does not require a spin excitation. For  $V > V_0$  (peak II) the spin-up Zeeman levels are in resonance and can generate a tunneling current. If a spin-down electron enters the left quantum dot, it blocks the single-electron tunneling current. This blockade can be lifted by a spin flip to the spin-up level with a rate  $\bar{\gamma}$ . However, its lifting requires spin excitation and, thus, is observed only at sufficiently high temperatures such that  $kT$  exceeds the Zeeman splitting. Therefore, we observe peak II at 1.5 K whereas at 100 mK it cannot be observed for magnetic fields larger than 0.5 T.

At this stage, it is worth emphasizing the difference to Ref. [30] where a similar level structure has been studied. There, the inter-dot tunneling  $\Omega$  is two orders of magnitude larger and comes close to the Zeeman splittings and exceeds the dot-lead couplings (in our setup by contrast,  $\Omega \ll \Gamma_{L,R}$ ). Then the spin-up as well as the spin-down states hybridize and form delocalized orbitals. When all levels are within the voltage window, this causes a current peak at  $V = V_0$  even in the absence of spin flips. By contrast, when  $\Omega$  is much smaller than the difference of the Zeeman splittings, we observe a blockade which is resolved by spin flips. Hence the current peaks provide information on the spin-flip rates.

The color graphs in Fig. 2(a) show the current as a function of the bias voltage and the magnetic field for various temperatures, where a magnetic field  $B_{\parallel}$  was applied parallel to the current (perpendicular to the layer structure). The observed oscillations and shifts with magnetic field originate from the Landau-level structure in the emitter. Nevertheless, the peak-to-peak distances of the double peak increase more or less linearly with the magnetic field as shown in Fig. 2(b), where the position of peak II is shown relative to the position of peak I. In the same way in Fig. 2(b) also the results for the other magnetic field direction are shown. In both cases, the observed difference in peak positions is given by

$$\Delta V = |g_L - g_R| \mu_B B / \eta, \quad (1)$$

with the gyromagnetic ratio  $g_{\ell}$  of quantum dot  $\ell = L, R$  and the leverage factor  $\eta$ . The individual Zeeman splittings  $g_{\ell} \mu_B B$

of the two dots do not appear, only the difference  $\Delta g = g_L - g_R$  plays a role here. Taking into account the leverage factor of  $\eta = 0.15$  we obtain for  $B_\perp$  a difference in the Landé factors  $\Delta g = 0.85$ , whereas for  $B_\parallel$  the value is  $\Delta g = 1$ . Anisotropy of the g-factor is well known for single InAs quantum dots [39–42]. Thus, the observed difference in  $\Delta g$  for the different magnetic field directions can be attributed to the anisotropy of the g-factors of the individual quantum dots.

### III. DOUBLE QUANTUM DOT-ENVIRONMENT MODEL

For a theoretical description of our observations, we start with the model used in Ref. [31] and also consider spin-flip cotunneling [6, 7]. In doing so, we model each quantum dot with a single level with onsite energy  $\epsilon_\ell$  ( $\ell = L, R$ ) and tunnel coupling  $\Omega$ . In the operating regime of our experiment, Coulomb repulsion allows the occupation of the double quantum dot with only one electron. Dot  $L$  is tunnel coupled also to an electron source from which electrons may enter at rate  $\Gamma_L$ . Correspondingly, dot  $R$  is coupled to a drain with rate  $\Gamma_R$ . The broadening of the current peaks with increasing temperature can be explained by the coupling of the double quantum dot dipole moment to a bosonic heat bath [32, 33, 43] with ohmic spectral density and a dimensionless coupling strength  $\alpha$ . For details see Ref. [31].

Spin flips may be treated at different levels ranging from a phenomenological Lindblad master equation to microscopic models for spin-orbit interaction and the hyperfine interaction with the magnetic moments in the substrate. Such models may predict characteristic dependencies of the decay rates on the Zeeman splitting. In turn, measurements of the spin-flip rates hint on the dominating mechanism. In the present case, a model must be capable of explaining the significant temperature dependence and the observed increase of the spin-flip rate with the Zeeman splitting. Moreover, it must provide the asymmetry between spin decay and thermal excitation.

These requirements can be fulfilled by spin-flip cotunneling [6, 7] induced by the spin-conserving tunnel Hamiltonian  $H_T = \sum_{k\sigma} t_k (c_{k\sigma}^\dagger d_\sigma + d_\sigma^\dagger c_{k\sigma})$ , where the fermionic operators  $c_{k\sigma}$  and  $d_\sigma$  annihilate an electron with spin  $\sigma$  in the left lead and the left dot, respectively (spin flips in the right dot do not play a role and will be ignored). In a  $T$ -matrix formulation, the impact of  $H_T$  is given by an effective coupling that obeys the recursive relation  $T = H_T + H_T G_0(E_i) T$ , where  $G_0(z) = (z - H_0)^{-1}$  is the Green function in the absence of tunneling and  $E_i$  the energy of the initial state [44].

Our focus lies on spin flips in a singly occupied quantum dot, where Coulomb repulsion and Pauli principle forbid resonant dot-lead tunneling, such that the leading contribution to  $T$  is the second-order term  $H_T G_0 H_T$  which causes the process schematically shown in Fig. 3(a). A spin-up electron flips to the lower Zeeman level, while a lead electron at the Fermi surface is excited. The opposite process requires the decay of a lead electron, which is possible only at sufficiently high temperature. The virtually populated dot states of this second-order process are the empty dot and the singlet state. In the Appendix, we show that the  $T$ -matrix can be approxi-

mated as  $T = \hbar(\sigma_\uparrow^\dagger \sigma_\downarrow \zeta + \sigma_\downarrow^\dagger \sigma_\uparrow \zeta^\dagger)$ , where  $\zeta$  describes quantum noise stemming from electron excitations under spin-flip at the Fermi surface of the lead. For the numerical treatment, we employ a Bloch-Redfield master equation [45, 46]. The dissipative kernel stemming from  $T$  is fully specified by the noise correlation  $C(t) = \langle \zeta(0) \zeta^\dagger(t) \rangle$  which in frequency space reads  $C(\omega) = \pi \alpha_{\text{spin}} \omega n_{\text{th}}(\hbar\omega)$  with the Bose function  $n_{\text{th}}(E) = [\exp(E/kT) - 1]^{-1}$ . While the order of magnitude of the dimensionless dissipation strength  $\alpha_{\text{spin}}$  can be estimated from the dot-lead coupling  $\Gamma_L$ , the onsite interaction, and the chemical potential, we will determine its precise value by fitting our experimental data. Details of the derivation and the relation to the ohmic spin-boson model are provided in the Appendix.

Before focussing on spin flips, we consider the current peaks in the absence of the magnetic field shown in Fig. 3(b). Proceeding as in Ref. [31], we determine the dot-lead rates  $\Gamma_{L/R}$ , the inter-dot tunneling  $\Omega$ , and the dimensionless dissipation strength  $\alpha$  of the orbital degree of freedom to  $\Omega = 0.85 \mu\text{eV}$ ,  $\Gamma_R = 5 \mu\text{eV}$ ,  $\alpha = 0.005$ . Due to the asymmetric coupling,  $\Gamma_R \ll \Gamma_L$  while the value of  $\Gamma_L$  does not greatly influence the current. In comparison to the dots studied in Ref. [30] this is two orders of magnitude smaller inter-dot tunneling and even in comparison to the resonance peaks studied in Ref. [31] the inter-dot tunneling is a factor of 2 (peak II in Ref. [31]) to 5 (peak I) smaller, i.e. indicating a very weak coupling between the two dots in the work here.

To analyze the spin flips, we focus on the peaks whose position and height changes with the magnetic field. Figure 3(c) shows the two peaks for a magnetic field  $B_\perp = 1.1 \text{ T}$  and two different temperatures. In the further analysis the height of the peaks is analyzed as function of the magnetic field, i.e., the peak position on the voltage axes relative to  $V_0$ . In this way Fig. 3(d) shows the height of the peaks as a function of their position for the two different temperatures (red circles:  $T = 1.5 \text{ K}$ , blue triangles:  $T = 0.1 \text{ K}$ , where peak II vanishes for higher magnetic fields). In the Appendix we show that also for the parallel magnetic field direction similar results are obtained. Solving numerically our above model leads to two fitting parameters in addition to the parameters extracted for  $B = 0$  and in addition to  $\Delta g$  extracted from the observed Zeeman splitting. The two fitting parameters are the dimensionless spin dissipation  $\alpha_{\text{spin}} = 1.2 \times 10^{-4}$  and the gyromagnetic ratio of the left dot,  $g_L = 0.7$  (for  $B_\parallel$  we obtain  $g_L = 1$ ). Only  $g_L$  plays a role since our spin-blockade mechanism is governed by the spin relaxation in the left dot. The experimental results are well reproduced by our model (solid lines) in using these two fitting parameters for both temperatures. At a temperature of  $T = 1.5 \text{ K}$  the model describes the experimental results almost perfectly showing that our assumption of an ohmic spectral density is well justified. At a temperature of  $T = 0.1 \text{ K}$ , especially at more negative voltages (higher magnetic fields) deviations between theory and experiment are observed. These deviations might be caused by the influence of noise on the very sharp peaks (see the Appendix for our analysis of the noise in the signal). Nevertheless, also at this low temperature our theoretical model describes the experimental results rather well. The dimensionless spin dissipation  $\alpha_{\text{spin}}$  which we ob-

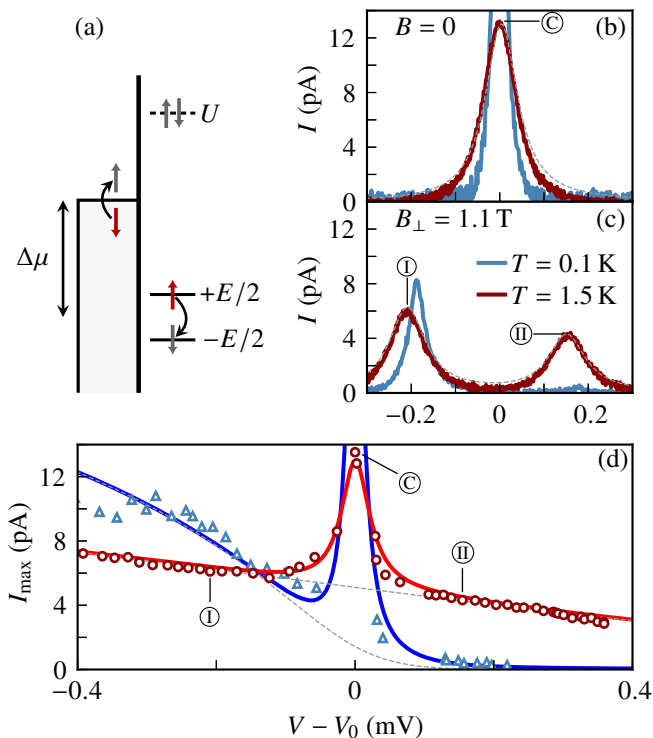


FIG. 3. (a) Spin dissipation due to cotunneling. (b,c) Measured tunneling current as a function of the bias voltage in the absence ( $B = 0$ ) and presence ( $B_{\perp} = 1.1$  T) of a magnetic field, respectively, for temperatures  $T = 100$  mK and  $T = 1.5$  K. The resonance peaks are centered around the peak position  $V_0$  at  $B = 0$ . The dashed line indicates the numerical data for the higher temperature with  $\Omega = 0.85$   $\mu$ eV,  $\Gamma_R = 5$   $\mu$ eV,  $\alpha = 0.005$ ,  $\alpha_{\text{spin}} = 1.2 \times 10^{-4}$ , and  $g_L = 0.7$ . (d) Corresponding peak heights as a function of the bias voltage. Symbols mark the experimental values, while the solid lines indicate numerical data. The dotted lines outline the analytical approximation in Eq. (2).

tained from fitting our model is our central quantity of interest, because it allows predictions for the spin coherence [47, 48]. The good description of the experimental results by our model clearly hints towards spin-flip cotunneling as the main process in our system.

#### IV. ENERGY DEPENDENCE OF THE SPIN DECAY

While we have seen that the spin-flip cotunneling predicts the behaviour in the magnetic field rather well, we now aim at a more direct access to the spin-flip rate as a function of the Zeeman splitting. For this purpose, we capture the scenario of the spin blockade by a rate equation which holds for sufficiently large magnetic field such that the two peaks are well separated. We assume that an electron with arbitrary spin orientation enters from the source to the left dot, where it undergoes spin flips with the spin decay rate  $\gamma$  and the corresponding thermal excitation rate  $\bar{\gamma}$ . Both rates are assumed to be linked by the detailed balance relation  $\bar{\gamma}(E)/\gamma(E) = \exp(-E/kT)$ . At the peak, one Zeeman level is in resonance with the corresponding

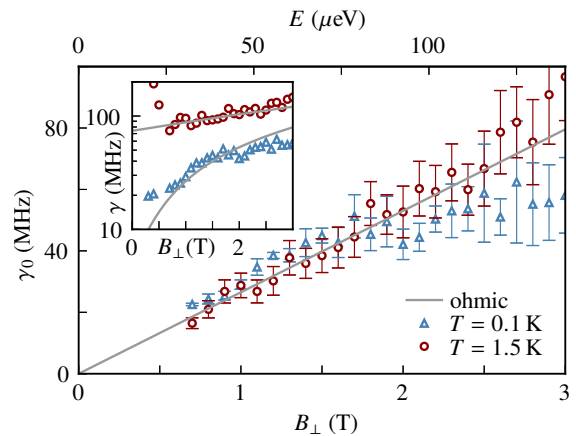


FIG. 4. Spin-flip rate in the zero-temperature limit,  $\gamma_0$ , as a function of the Zeeman splitting (upper axis) and the corresponding magnetic field. The values are obtained from the approximate analytical solution in Eq. (2) together with the detailed-balance relation. For the size of the error bars, see the Appendix. Inset: Spin-flip rate at finite temperature,  $\gamma(E) = \gamma_0(E)[1 + n_{\text{th}}(E)]$ .

level of the right dot, the electron may proceed to the drain with some effective rate  $\Gamma_{\text{eff}}$ . The resulting rate equation provides the current

$$I(B) = \frac{2\gamma I_0}{I_0/e + 2\gamma + 2\bar{\gamma}} \quad (2)$$

with  $I_0$  the peak height at zero magnetic field and the Zeeman splitting in the left dot,  $E = g_L \mu_B B$ . Interestingly, for sufficiently large  $g_L$ , this result depends on  $\Omega$  and  $\Gamma_R$  only via  $I_0$ .

Equation (2) together with the detailed balance relation provides  $\gamma$  as a function of the Zeeman splitting  $E$  and  $I_0$ . At low temperatures, the result corresponds to the spontaneous decay rate. Moreover, under the assumption that the induced decay is proportional to the thermal occupation of the environmental modes  $n_{\text{th}}(E) = [\exp(E/kT) - 1]^{-1}$ , we may compute the spontaneous decay rate also from measurements at higher temperatures. Therefore, we conjecture that  $\gamma_0(E) \equiv \gamma(E)/[1 + n_{\text{th}}(E)]$  is temperature independent and grows linearly with the Zeeman splitting and, hence, with the magnetic field. Figure (4) shows the accordingly evaluated experimental data. They show a good agreement for  $B_{\perp} \gtrsim 0.5$  T, while below this value, the peaks overlap such that Eq. (2) does not hold. Especially for  $T = 1.5$  K the agreement is quite good. One obtains spin relaxation rates varying between 20 MHz at 0.7 T and about 80 MHz at 3 T. This linear behaviour is directly related to the ohmic spectral density and supports our conjecture of spin-flip cotunneling resolving the current blockade. At  $T = 100$  mK, one witnesses a deviation which we attribute to the already mentioned underestimation of the peak height. Moreover, for large Zeeman splittings, the thermal excitation rate becomes small, which augments the relative error.

In principle, one may consider other spin-dissipation mechanisms such as spin-orbit or hyperfine interaction. These, however, are expected to show a stronger dependence on the

magnetic field and can be ruled out. A further conceivable mechanism to resolve the blockade is dissipative transitions from the left to the right dot [31]. As such transitions occur also when both Zeeman levels are misaligned, they cannot explain the emergence of sharp resonance peaks with the observed asymmetry.

## V. CONCLUSIONS

We have used a spin-dependent blockade mechanism for single electrons in self-assembled double quantum dots to extract spin relaxation rates directly from the measured resonant tunnel currents. The blockade mechanism here stems from inhomogeneous Zeeman splittings such that the two spin channels are never resonant simultaneously. Then an electron in the off-resonant channel blocks transport until a spin flip occurs. An analysis based on a rate equation provided the spin-flip rates which turned out to grow linearly with the Zeeman splitting. Quantitatively, the spontaneous spin decay rate at 2 T is of the order 50 MHz. Hence, we expect coherence times of roughly 20 ns which corresponds to a few hundred coherent oscillations. The here discussed findings identify spin-flip cotunneling as the dominating decoherence mechanism.

## ACKNOWLEDGMENTS

This work was supported by the Deutsche Forschungsgemeinschaft (DFG, German Research Foundation) under Germany's Excellence Strategy – EXC 2123 QuantumFrontiers – 390837967, the State of Lower Saxony of Germany via the Hannover School for Nanotechnology, and by the Spanish Ministry of Science, Innovation, and Universities (Grant No. PID2020-117787GB-I00), and by the CSIC Research Platform on Quantum Technologies PTI-001.

## APPENDIX A: DATA ANALYSIS

### 1. Position, height, and width of the peaks

The data analysis of the experimental current-voltage characteristics consists in a first step in the subtraction of the background. Therefore, the left and right background to each resonance are exponentially fitted and the fits are stitched together at their intersection. The combined background is then subtracted from the raw current-voltage characteristics. We refer to these resulting background-less data shortly as measured data.

To determine the peak height and position we explore the influence of the noise in the signal. We start by filtering the signal using a Savitzky-Golay filter [49] and then subtract the filtered signal from the measured data as shown in Fig. 5. The standard deviation of the resulting data points is converted and represented by the error bars in Fig. 4 in the main text. At the low temperature of  $T = 0.1$  K and higher magnetic fields, the peaks become very sharp [Fig. 5(e)] such that at

the peak position, the deviation of the filtered signal from the measurement is much larger than the noise, see inset in Fig. 5(e). Therefore the sharp peak is taken into account in the size of the error bars.

### 2. Fitting of the spin dissipation strength

In our data analysis, the detuning of the quantum dot (QD) levels is linked to the bias voltage via  $\epsilon = \eta V$ , where the leverage factor can be estimated from the assumed voltage drop across the sample as  $\eta \approx 0.15$ . To reveal the sensitivity of our fit parameters to the value of  $\eta$ , we show in the last line of Table I how the fit parameters to leading order depend on  $\eta$ . In particular the central quantity determined in this work, namely the dimensionless spin dissipation strength  $\alpha_{\text{spin}}$  is practically independent of the leverage.

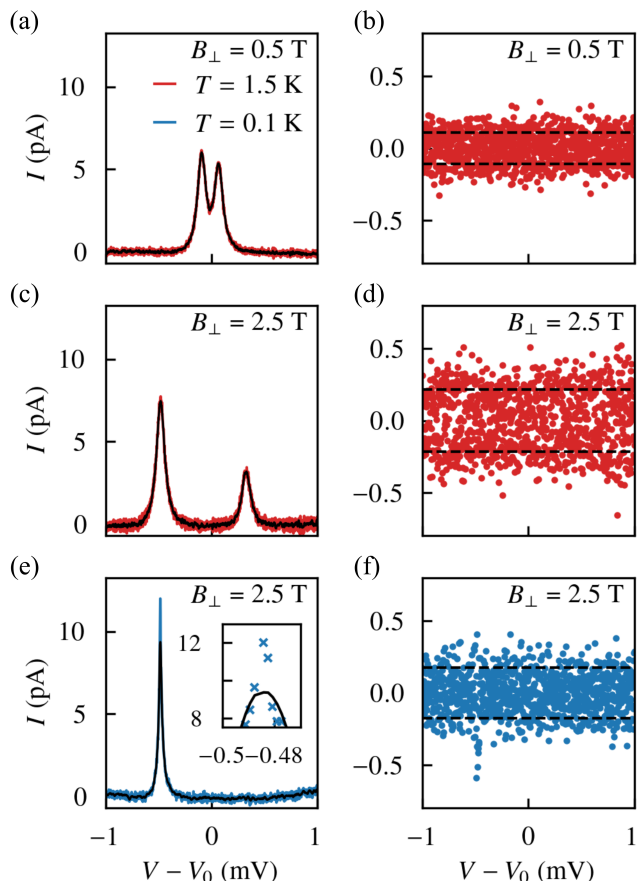


FIG. 5. (a,c) Measured tunneling current (red line) as a function of the bias voltage at a temperature of  $T = 1.5$  K for magnetic fields  $B_{\perp} = 0.5$  T and 2.5 T, respectively. The black line is the Savitzky-Golay filtered signal. (e) Same at  $T = 0.1$  K and  $B_{\perp} = 2.5$  T. The inset shows the peak in high resolution, while the blue lines and symbols mark measured data. (b,d,f) Difference of the measured data and the filtered signal. The dashed lines mark the range of the standard deviation.

TABLE I. Model parameters determined by fitting the experimental peak heights for the leverage factor  $\eta = 0.15$ . The last row shows the approximate dependence of the fit parameters on  $\eta$ . Remarkably, the fit value for the dimensionless spin dissipation strength  $\alpha_{\text{spin}}$  is practically independent of  $\eta$  and the orientation of the magnetic field.

	$\Gamma_R$ ( $\mu\text{eV}$ )	$\Omega$ ( $\mu\text{eV}$ )	$\alpha \times 10^3$	$\Delta g = g_R - g_L$	$g_L$	$\alpha_{\text{spin}} \times 10^4$
$B_{\perp}$	5	0.85	5.0	0.85	0.7	1.2
$B_{\parallel}$	5	0.85	5.0	1	1	1.2
	$\propto \eta$	$\propto \eta^{1/2}$	$\propto \eta$	$\propto \eta$	$\propto \eta^0$	$\propto \eta^0$

## APPENDIX B: MAGNETIC-FIELD DIRECTION DEPENDENCE

A magnetic field  $B_{\parallel}$  applied parallel to the tunneling current (i.e. perpendicular to the layer) induces oscillations in the current-voltage characteristics which are absent in the case of a perpendicular field  $B_{\perp}$  as is discussed in Figs. 1 and 2 of the

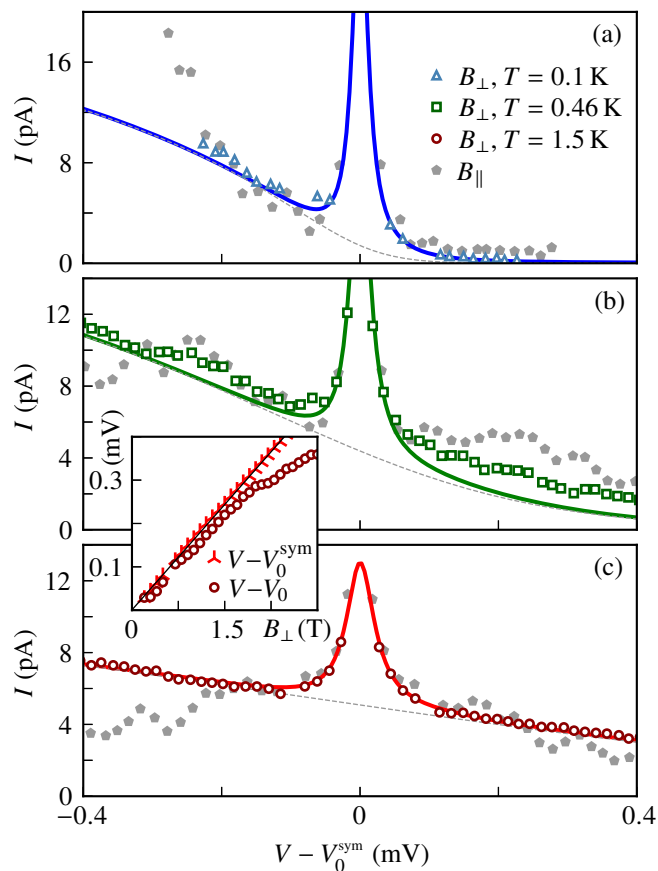


FIG. 6. Peak heights of the measured tunneling current as a function of the bias voltage for perpendicular (colored symbols) and parallel (gray symbols) applied magnetic field at temperature  $T = 0.1$  K (a),  $0.46$  K (b), and  $1.5$  K (c). The peak positions are taken with respect to the midpoint  $V_0^{\text{sym}}$  between the peaks. Solid and dashed lines, respectively, indicate the numerical data and the analytical approximation (D3) for the case of finite  $B_{\perp}$ . The inset shows the peak positions with respect to  $V_0^{\text{sym}}$  and the position  $V_0$  at zero magnetic field in dependence of  $B_{\perp}$  for  $T = 1.5$  K.

main text. Nevertheless, the peak-to-peak distance increases in both cases linearly with the magnetic field. We show in Fig. 6 that also the peak heights evolve overall quite similarly for both magnetic-field directions with the peak position when taking the midpoint  $V_0^{\text{sym}}$  between the two peaks as reference point. For consistency and in contrast to the main text, we here use also for perpendicular orientation  $V_0^{\text{sym}}$  as reference point. The inset of Fig. 6 shows that for  $B_{\perp} \lesssim 1.7$  T, the difference between  $V_0$  and  $V_0^{\text{sym}}$  is minor.

Upon closer look, one notices that for parallel magnetic field, Landau oscillations become apparent which for perpendicular magnetic-field direction is not the case. These Landau oscillations predominantly affect the density of states in the leads and are not captured by our theory, which explains the slightly larger deviation from the theoretical prediction in the presence of  $B_{\parallel}$ .

## APPENDIX C: OHMIC DISSIPATION FROM SPIN-FLIP COTUNNELING

The coupling of a spin to a bosonic heat bath can be written as  $V = \hbar\sigma_x\xi$  with the effective bath coordinate  $\xi = \sum_{\nu} \lambda_{\nu}(a_{\nu} + a_{\nu}^{\dagger})$ , where  $a_{\nu}$  is the usual bosonic annihilation operator of a bath mode with frequency  $\omega_{\nu}$  and the coupling energy  $\hbar\lambda_{\nu}$ . Its auto-correlation function  $C(t) = \langle \xi(0)\xi(t) \rangle$  contains all information about the bath needed to evaluate the dissipative terms of the Bloch-Redfield equation [45, 46]. For a Gibbs

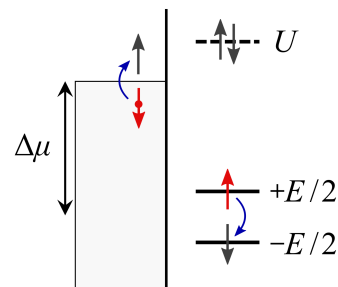


FIG. 7. Spin-flip cotunneling in a single quantum dot coupled to a lead. A dot electron initially in the upper Zeeman level (red) flips to the spin-down level (green), while in the leads a spin-down electron at the Fermi surface is excited under spin flip. The virtually populated dot states of this second-order process may be the empty dot or the singlet state which is separated from the singly occupied state by the interaction energy  $U$ .

state, in frequency space it reads

$$C(\omega) = 2J(\omega)n_{\text{th}}(\hbar\omega) \quad (\text{C1})$$

with the bath spectral density  $J(\omega) = \pi \sum_{\nu} |\lambda_{\nu}|^2 \delta(\omega - \omega_{\nu})$  and the bosonic thermal occupation number  $n_{\text{th}}(E) = [\exp(E/kT) - 1]^{-1}$ . In the following, we demonstrate that spin-flip cotunneling corresponds to quantum noise obeying the correlation (C1) with ohmic spectral density, i.e.,  $J(\omega) \propto \omega$ .

To this end, we employ ideas developed in the context of Pauli spin blockade in double quantum dots [6, 7]. Focussing on spin flips within a QD, we consider a single orbital with Zeeman splitting  $E$  coupled to a lead as is sketched in Fig. 7. We assume that the dot orbital lies significantly below the Fermi surface of the lead such that  $E \ll \Delta\mu, kT$ . Moreover, the intra-dot interaction  $U$  allows only virtual double occupation of the QD.

A convenient starting point is the  $T$ -matrix formulation of the dot-lead tunneling process for the tunneling Hamiltonian  $H_T = \sum_{k,\sigma} t_k (c_{k\sigma}^{\dagger} d_{\sigma} + d_{\sigma}^{\dagger} c_{k\sigma})$  for spin-conserving tunneling between the QD and the lead with the spin-independent matrix elements  $t_k$ . The corresponding electron annihilation operators are  $c_{k\sigma}$  and  $d_{\sigma}$ , where  $\sigma$  is the spin quantum number and  $k$  labels the lead orbitals. In the situation considered, the Pauli exclusion principle together with Coulomb repulsion does not allow resonant tunneling. Then the leading contribution of the  $T$ -matrix is the second-order term [7, 44]

$$T = H_T \frac{1}{E_i - H_0} H_T, \quad (\text{C2})$$

which replaces the tunnel Hamiltonian in the Bloch-Redfield equation and in the golden-rule rates. Here  $E_i$  is the energy of an initial state  $|i\rangle$  in the many-electron Hilbert space of QD and lead, while  $H_0$  is the Hamiltonian in the absence of tunneling. It has to be evaluated for the virtually occupied intermediate states  $|\nu\rangle$  created by  $H_T$ .

Following Ref. [7], we estimate  $E_i - H_0$  for the initial QD state  $|\uparrow\rangle$ . Its decay towards  $|\downarrow\rangle$  induced by  $H_T$  may occur via the intermediate states  $c_{k\uparrow}^{\dagger} d_{\uparrow} |i\rangle$  and  $d_{\downarrow}^{\dagger} c_{k\downarrow} |i\rangle$ , i.e., the empty and the doubly occupied QD. Since the total energy of the transition induced by  $T$  must be conserved, the necessary excitation of a lead electron can occur only at the Fermi surface. Therefore the energy differences of the initial state and the intermediate states are  $E_i - E_{\nu} = -\Delta\mu$  and  $E_i - E_{\nu} = -U$ , respectively, see Fig. 7. Hence the  $T$ -matrix can be approximated as

$$T = \hbar(d_{\downarrow}^{\dagger} d_{\downarrow} \zeta + d_{\uparrow}^{\dagger} d_{\uparrow} \zeta^{\dagger}) \quad (\text{C3})$$

with the (operator-valued) quantum noise

$$\zeta = \frac{1}{\hbar W} \sum_{k,k'} t_k t_{k'} c_{k\downarrow}^{\dagger} c_{k'\uparrow} \quad (\text{C4})$$

and the effective energy difference  $W$  defined via

$$\frac{1}{W} = \frac{1}{\Delta\mu} + \frac{1}{U}. \quad (\text{C5})$$

A straightforward calculation yields for a Gibbs state of the lead with spin-independent chemical potential  $\mu$  the correlation function

$$C_{\text{cot}}(t) = \langle \zeta^{\dagger}(0) \zeta(t) \rangle = \langle \zeta(0) \zeta^{\dagger}(t) \rangle \quad (\text{C6})$$

$$= \left( \frac{\Gamma}{2\pi\hbar W} \right)^2 \int d\epsilon d\epsilon' e^{-i(\epsilon - \epsilon')t/\hbar} \times f(\epsilon - \mu) [1 - f(\epsilon' - \mu)] \quad (\text{C7})$$

with the Fermi function  $f(E) = [\exp(E/kT) + 1]^{-1}$ . In a continuum approximation, we have defined  $\Gamma = 2\pi \sum_k |t_k|^2 \delta(\epsilon - \epsilon_k)$ , where here  $\Gamma/\hbar$  is the dot-lead tunnel rate at the Fermi surface. By substituting  $\epsilon \rightarrow \hbar\omega + \epsilon'$  and evaluating the  $\epsilon'$ -integral, we obtain the auto-correlation in frequency space reading

$$C_{\text{spin}}(\omega) = \pi \alpha_{\text{spin}} \omega n_{\text{th}}(\hbar\omega), \quad (\text{C8})$$

with the dimensionless spin-dissipation strength

$$\alpha_{\text{spin}} = \left( \frac{\Gamma}{\pi W} \right)^2. \quad (\text{C9})$$

Thus the quantum noise entailed by cotunneling on a spin has the second-order correlation of a bosonic heat bath with ohmic spectral density  $J_{\text{spin}}(\omega) = \pi \alpha_{\text{spin}} \omega / 2$ .

The coupling operator (C3) between the spin and the noise together with the correlation function (C8) allows us to evaluate the dissipation kernel of the Bloch-Redfield equation, such that spin-flip cotunneling can be treated numerically. Moreover, it provides the spin decay rate [47, 48]

$$\gamma(E) = \frac{\pi}{\hbar} \alpha_{\text{spin}} E [n_{\text{th}}(E) + 1] \quad (\text{C10})$$

with the Zeeman splitting  $E = g\mu_B B$  and the Bohr magneton  $\mu_B$ . The corresponding thermal excitation rate  $\bar{\gamma}(E) = \gamma(E) \exp(-E/kT)$  obeys the detailed-balance relation between emission and absorption.

As discussed in the main text, our experimental results are compatible with a dissipation strength of the order  $\alpha_{\text{spin}} \sim 10^{-4}$ , which results from Eqs. (C5) and (C9) for the quite realistic values  $\Gamma = 100 \mu\text{eV}$  and  $U \approx \Delta\mu \approx 1.5 \text{ meV}$ . In experiments with (almost) closed QDs,  $\Gamma$  and hence  $\alpha_{\text{spin}}$  may be significantly smaller, such that spin decoherence is governed by other mechanisms such as hyperfine interaction.

Since  $\zeta \neq \zeta^{\dagger}$ , the  $T$ -matrix in Eq. (C3) is not exactly of the form as in the spin-boson model, which is  $\propto \sigma_x \xi$  with the hermitian operator-valued noise  $\xi$ . Therefore, we introduce the hermitian and statistically independent noise operators  $\xi_x = (\zeta^{\dagger} + \zeta)/2$  and  $\xi_y = (\zeta^{\dagger} - \zeta)/2i$ . Their auto-correlation function is also of the form (C1) with  $J(\omega) = \pi \alpha_{\text{spin}} \omega / 4$ . Then the  $T$ -matrix (concisely written with Pauli matrices  $\sigma_{\pm} = d_{\downarrow}^{\dagger} d_{\downarrow} = \sigma_{\downarrow}^{\dagger}$ ) becomes

$$T = \sigma_{-} \zeta^{\dagger} + \sigma_{+} \zeta = \sigma_x \xi_x + \sigma_y \xi_y. \quad (\text{C11})$$

This implies that on the level of Bloch-Redfield theory, spin-flip cotunneling causes the same spin dissipation as two equal bosonic heat baths coupled with strength  $\alpha_{\text{spin}}/2$  via  $\sigma_x$  and  $\sigma_y$ , respectively. We have verified that coupling to either bath with double strength yields the practically same results for the current.

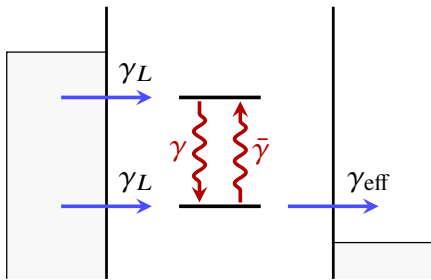


FIG. 8. Effective model underlying the rate equation (D1). The right QD and the drain are replaced by an effective depletion rate  $\gamma_{\text{eff}}$  for the lower Zeeman level, while the upper Zeeman level is not directly connected to the drain. The dissipative spin dynamics is captured by incoherent spin flips, while coherences are neglected.

#### APPENDIX D: ANALYTICAL APPROXIMATION

To obtain an analytical approximation for current, we derive a rate equation in which the tunneling from the left QD to the right QD and from there to the drain is replaced by an effective rate. Together with the spin-flip rates  $\gamma$  and  $\bar{\gamma}$ , this provides the result visualized in Fig. 6 by dashed lines.

When the Zeeman levels of the spin-down electrons on both QDs are aligned, an electron with this spin projection entering from the source can resonantly tunnel to the drain with some effective rate  $\gamma_{\text{eff}}$ . By contrast, a spin-up electron will get stuck in the left QD. Owing to Coulomb repulsion, it blocks the resonant spin-down channel. This blockade can be resolved by a spin flip which we assume to happen with a rate  $\gamma$ . Once

the electron is in the spin-down channel, we are back to the former situation. For consistency, we also have to take into account thermal spin excitation from the lower Zeeman level to the upper one, which occurs with rate  $\bar{\gamma}$ .

This scenario is sketched in Fig. 8 and can be described by the master equation

$$\frac{d}{dt} \begin{pmatrix} p_0 \\ p_\uparrow \\ p_\downarrow \end{pmatrix} = \begin{pmatrix} -2\gamma_L & 0 & \gamma_{\text{eff}} \\ \gamma_L & -\gamma & \bar{\gamma} \\ \gamma_L & \gamma & -\bar{\gamma} - \gamma_{\text{eff}} \end{pmatrix} \begin{pmatrix} p_0 \\ p_\uparrow \\ p_\downarrow \end{pmatrix}, \quad (\text{D1})$$

where  $\gamma_L = \Gamma_L/\hbar$ . The current is given by the population of the lower Zeeman level times the effective decay rate to the drain,

$$I = e\gamma_{\text{eff}} p_\downarrow. \quad (\text{D2})$$

In the absence of the spin-up channel, the physical situation is that of spin independent transport. Therefore, we can identify the corresponding current with the one in the absence of the magnetic field,  $I_0 = e\gamma_{\text{eff}}$ . It is straightforward to obtain  $p_\downarrow$  from the master equation (D1), such that in the limit  $\gamma_L \gg \gamma, \bar{\gamma}, \gamma_{\text{eff}}$ , the current reads

$$I = \frac{2\gamma I_0}{I_0/e + 2\gamma + 2\bar{\gamma}}. \quad (\text{D3})$$

Since we have assumed clearly distinct Zeeman levels, this result holds only when the peaks for the two spin channels do not overlap, i.e., far from the central peak at  $B = 0$ . Interestingly, this expression does not depend on the effective tunnel rate to the drain,  $\gamma_{\text{eff}}$ .

- 
- [1] D. Loss and D. P. DiVincenzo, Quantum computation with quantum dots, *Phys. Rev. A* **57**, 120 (1998).
  - [2] A. J. Weinstein, M. D. Reed, A. M. Jones, R. W. Andrews, D. Barnes, J. Z. Blumoff, L. E. Euliss, K. Eng, B. H. Fong, S. D. Ha, D. R. Hulbert, C. A. C. Jackson, M. Jura, T. E. Keating, J. Kerckhoff, A. A. Kiselev, J. Matten, G. Sabbir, A. Smith, J. Wright, M. T. Rakher, T. D. Ladd, and M. G. Borselli, Universal logic with encoded spin qubits in silicon, *Nature (London)* **615**, 817 (2023).
  - [3] W. Gilbert, T. Tanttu, W. H. Lim, M. Feng, J. Y. Huang, J. D. Cifuentes, S. Serrano, P. Y. Mai, R. C. C. Leon, C. C. Escott, K. M. Itoh, N. V. Abrosimov, H.-J. Pohl, M. L. W. Thewalt, F. E. Hudson, A. Morello, A. Laucht, C. H. Yang, A. Saraiva, and A. S. Dzurak, On-demand electrical control of spin qubits, *Nat. Nanotechn.* **18**, 131 (2023).
  - [4] G. Burkard, T. D. Ladd, A. Pan, J. M. Nichol, and J. R. Petta, Semiconductor spin qubits, *Rev. Mod. Phys.* **95**, 025003 (2023).
  - [5] J. Schliemann, A. V. Khaetskii, and D. Loss, Spin decay and quantum parallelism, *Phys. Rev. B* **66**, 245303 (2002).
  - [6] F. Qassemi, W. A. Coish, and F. K. Wilhelm, Stationary and transient leakage current in the pauli spin blockade, *Phys. Rev. Lett.* **102**, 176806 (2009).
  - [7] W. A. Coish and F. Qassemi, Leakage-current line shapes from inelastic cotunneling in the pauli spin blockade regime, *Phys. Rev. B* **84**, 245407 (2011).
  - [8] W. A. Coish, J. Fischer, and D. Loss, Exponential decay in a spin bath, *Phys. Rev. B* **77**, 125329 (2008).
  - [9] W. A. Coish and D. Loss, Hyperfine interaction in a quantum dot: Non-Markovian electron spin dynamics, *Phys. Rev. B* **70**, 195340 (2004).
  - [10] R. Hanson, B. Witkamp, L. M. K. Vandersypen, L. H. W. van Beveren, J. M. Elzerman, and L. P. Kouwenhoven, Zeeman energy and spin relaxation in a one-electron quantum dot, *Phys. Rev. Lett.* **91**, 196802 (2003).
  - [11] J. M. Elzerman, R. Hanson, L. H. W. v. Beveren, B. Witkamp, L. M. K. Vandersypen, and L. P. Kouwenhoven, Single-shot read-out of an individual electron spin in a quantum dot, *Nature (London)* **430**, 431 (2004).
  - [12] S. Amasha, K. MacLean, I. P. Radu, D. M. Zumbühl, M. A. Kastner, M. P. Hanson, and A. C. Gossard, Electrical control of spin relaxation in a quantum dot, *Phys. Rev. Lett.* **100**, 046803 (2008).
  - [13] L. C. Camenzind, L. Yu, P. Stano, J. D. Zimmermann, A. C. Gossard, D. Loss, and D. M. Zumbühl, Hyperfine-phonon spin relaxation in a single-electron GaAs quantum dot, *Nature Commun.* **9**, 3454 (2018).
  - [14] A. Kurzmann, P. Stegmann, J. Kerski, R. Schott, A. Ludwig, A. D. Wieck, J. König, A. Lorke, and M. Geller, Optical detection of single-electron tunneling into a semiconductor quantum dot, *Phys. Rev. Lett.* **122**, 247403 (2019).



- [15] L. Banszerus, K. Hecker, S. Möller, E. Icking, K. Watanabe, T. Taniguchi, C. Volk, and C. Stampfer, Spin relaxation in a single-electron graphene quantum dot, *Nature Commun.* **13**, 3637 (2022).
- [16] K. Ono, D. G. Austing, Y. Tokura, and S. Tarucha, Current rectification by Pauli exclusion in a weakly coupled double quantum dot system, *Science* **297**, 1313 (2002).
- [17] A. C. Johnson, J. R. Petta, J. M. Taylor, A. Yacoby, M. D. Lukin, C. M. Marcus, M. P. Hanson, and A. C. Gossard, Triplet-singlet spin relaxation via nuclei in a double quantum dot, *Nature (London)* **435**, 925 (2005).
- [18] F. H. L. Koppens, K. C. Nowack, and L. M. K. Vandersypen, Spin echo of a single electron spin in a quantum dot, *Phys. Rev. Lett.* **100**, 236802 (2008).
- [19] H. Bluhm, S. Foletti, I. Neder, M. Rudner, D. Mahalu, V. Umansky, and A. Yacoby, Dephasing time of GaAs electron-spin qubits coupled to a nuclear bath exceeding  $200\mu\text{s}$ , *Nature Phys.* **7**, 109 (2011).
- [20] V. Srinivasa, K. C. Nowack, M. Shafiei, L. M. K. Vandersypen, and J. M. Taylor, Simultaneous spin-charge relaxation in double quantum dots, *Phys. Rev. Lett.* **110**, 196803 (2013).
- [21] V. F. Maisi, A. Hofmann, M. Rössli, J. Basset, C. Reichl, W. Wegscheider, T. Ihn, and K. Ensslin, Spin-orbit coupling at the level of a single electron, *Phys. Rev. Lett.* **116**, 136803 (2016).
- [22] S. Nadj-Perge, S. M. Frolov, E. P. A. M. Bakkers, and L. P. Kouwenhoven, Spin-orbit qubit in a semiconductor nanowire, *Nature (London)* **468**, 1084 (2010).
- [23] J.-Y. Wang, G.-Y. Huang, S. Huang, J. Xue, D. Pan, J. Zhao, and H. Xu, Anisotropic Pauli spin-blockade effect and spin-orbit interaction field in an InAs nanowire double quantum dot, *Nano Lett.* **18**, 4741 (2018).
- [24] M. D. Schroer, K. D. Petersson, M. Jung, and J. R. Petta, Field tuning the  $g$  factor in InAs nanowire double quantum dots, *Phys. Rev. Lett.* **107**, 176811 (2011).
- [25] N. S. Lai, W. H. Lim, C. H. Yang, F. A. Zwanenburger, W. A. Coish, F. Qassemi, A. Morello, and A. S. Dzurak, Pauli spin blockade in a highly tunable silicon double quantum dot, *Sci. Rep.* **1**, 110 (2011).
- [26] G. Yamahata, T. Koder, H. O. H. Churchill, K. Uchida, C. M. Marcus, and S. Oda, Magnetic field dependence of pauli spin blockade: A window into the sources of spin relaxation in silicon quantum dots, *Phys. Rev. B* **86**, 115322 (2012).
- [27] R. Li, F. E. Hudson, A. S. Dzurak, and A. R. Hamilton, Pauli spin blockade of heavy holes in a silicon double quantum dot, *Nano Lett.* **15**, 7314 (2015).
- [28] M. Brauns, J. Ridderbos, A. Li, E. P. A. M. Bakkers, W. G. van der Wiel, and F. A. Zwanenburger, Anisotropic pauli spin blockade in hole quantum dots, *Phys. Rev. B* **94**, 041411 (2016).
- [29] T. Zhang, H. Liu, F. Gao, G. Xu, K. Wang, X. Zhang, G. Cao, T. Wang, J. Zhang, X. Hu, H.-O. Li, and P. Guo, Anisotropic  $g$ -factor and spin-orbit field in a germanium hut wire double quantum dot, *Nano Lett.* **21**, 3835 (2021).
- [30] S. M. Huang, Y. Tokura, H. Akimoto, K. Kono, J. J. Lin, S. Tarucha, and K. Ono, Spin bottleneck in resonant tunneling through double quantum dots with different zeeman splittings, *Phys. Rev. Lett.* **104**, 136801 (2010).
- [31] O. Dani, R. Hussein, J. C. Bayer, S. Kohler, and R. J. Haug, Temperature-dependent broadening of coherent current peaks in InAs double quantum dots, *Commun. Phys.* **5**, 292 (2022).
- [32] A. J. Leggett, S. Chakravarty, A. T. Dorsey, M. P. A. Fisher, A. Garg, and W. Zwerger, Dynamics of the dissipative two-state system, *Rev. Mod. Phys.* **59**, 1 (1987).
- [33] P. Hänggi, P. Talkner, and M. Borkovec, Reaction-rate theory: Fifty years after Kramers, *Rev. Mod. Phys.* **62**, 251 (1990).
- [34] Q. Xie, A. Madhukar, P. Chen, and N. P. Kobayashi, Vertically Self-Organized InAs Quantum Box Islands on GaAs(100), *Phys. Rev. Lett.* **75**, 2542 (1995).
- [35] H. Eisele, O. Flebbe, T. Kalka, C. Preinesberger, F. Heinrichsdorff, A. Krost, D. Bimberg, and M. Dähne-Prietsch, Cross-sectional scanning-tunneling microscopy of stacked InAs quantum dots, *Appl. Phys. Lett.* **75**, 106 (1999).
- [36] P. Barthold, F. Hohls, N. Maire, K. Pierz, and R. J. Haug, Enhanced shot noise in tunneling through a stack of coupled quantum dots, *Phys. Rev. Lett.* **96**, 246804 (2006).
- [37] G. Kießlich, E. Schöll, T. Brandes, F. Hohls, and R. J. Haug, Noise enhancement due to quantum coherence in coupled quantum dots, *Phys. Rev. Lett.* **99**, 206602 (2007).
- [38] M. T. Björk, A. Fuhrer, A. E. Hansen, M. W. Larsson, L. E. Fröberg, and L. Samuelson, Tunable effective  $g$  factor in InAs nanowire quantum dots, *Phys. Rev. B* **72**, 201307 (2005).
- [39] I. Hapke-Wurst, U. Zeitler, R. J. Haug, and K. Pierz, Mapping the  $g$ -factor anisotropy of InAs self-assembled quantum dots, *Physica E* **12**, 802 (2002).
- [40] J. M. Meyer, I. Hapke-Wurst, U. Zeitler, R. J. Haug, and K. Pierz, Resonant tunneling through InAs quantum dots in tilted magnetic fields: experimental determination of the  $g$ -factor anisotropy, *Phys. Stat. Sol. B* **224**, 685 (2001).
- [41] A. Schwan, B.-M. Meiners, A. Greilich, D. R. Yakovlev, M. Bayer, A. D. B. Maia, A. A. Quivy, and A. B. Henriques, Anisotropy of electron and hole  $g$ -factors in (In,Ga)As quantum dots, *Appl. Phys. Lett.* **99**, 221914 (2011).
- [42] V. V. Belykh, D. R. Yakovlev, J. J. Schindler, E. A. Zhukov, M. A. Semina, M. Yacob, J. P. Reithmaier, M. Benyoucef, and M. Bayer, Large anisotropy of electron and hole  $g$ -factors in infrared-emitting InAs/InAlGaAs self-assembled quantum dots, *Phys. Rev. B* **93**, 125302 (2016).
- [43] U. Weiss, *Quantum Dissipative Systems*, 4th ed. (World Scientific, Singapore, 2012).
- [44] H. Bruus and K. Flensberg, *Many-Body Quantum Theory in Condensed Matter Physics* (Oxford University Press, New York, 2004).
- [45] A. G. Redfield, On the theory of relaxation processes, *IBM J. Res. Develop.* **1**, 19 (1957).
- [46] K. Blum, *Density Matrix Theory and Applications*, 2nd ed. (Springer, New York, 1996).
- [47] U. Weiss and M. Wollensak, Dynamics of the biased two-level system in metals, *Phys. Rev. Lett.* **62**, 1663 (1989).
- [48] Y. Makhlin, G. Schön, and A. Shnirman, Quantum-state engineering with Josephson-junction devices, *Rev. Mod. Phys.* **73**, 357 (2001).
- [49] A. Savitzky and M. J. E. Golay, Smoothing and differentiation of data by simplified least squares procedures, *Anal. Chem.* **36**, 1627 (1964).